Electronic Supplementary Material (ESI) for Physical Chemistry Chemical Physics.

Supplementary Information:

Understanding Mechanism and Kinetics of Formation and Breaking of Ring Structures During Silica Polymerization: A Computational Study

Inderdip Shere and **Ateeque Malani***

Department of Chemical Engineering, Indian Institute of Technology Bombay, Mumbai, India

(Corresponding author: amalani@iitb.ac.in)

Sections

Figures

Tables

S1 Silica Model and Force-field

We represent silica precursor by the tetrahedron, where silicon atom is at the center, and four hydroxyl (OH) groups are represented by the vertexes of the tetrahedron. The harmonic bond potential is applied between the vertexes to maintain the shape of the tetrahedron as,

$$U_B = \frac{K_B}{2} \sum_{i=1}^{4} \sum_{j=i+1}^{4} \left(|\mathbf{r}_i - \mathbf{r}_j| - r_0 \right)^2 , \tag{S1}$$

where, $\mathbf{r}_i$ is the position vector of i^{th} OH group, r_0 is the equilibrium distance, and K_B is harmonic strength. Hard-sphere interaction between silicon atoms were applied to prevents the unrealistic overlapping of the tetrahedrons. Overlapping of the vertices of two and more tetrahedrons are allowed and are desirable during condensation reaction. The angle between two connected tetrahedrons is maintained by harmonic angle potential,

$$U_A = \frac{K_A}{2} \left(\cos\theta - \cos\theta_0 \right)^2 , \tag{S2}$$

where, θ is the Si-O-Si angle, θ_0 is an equilibrium angle, and K_A is the strength of potential. The force-field parameters used are discussed in detail in our previous work[1–3] and tabulated here in Table S1. All simulations were performed in triplicates and data for one of the system is given in main manuscript and remaining two system is presented here.

Table S1: Force-field parameters

Property	$\mathrm{r_{HS}}$ (Å)	$\mathrm{r_0}$ (Å)	θ_0 (deg)	K_B (kJ mol^{-1}Å^{-2})	K_A (kJ mol^{-1})	K_{eq}
Values	2	2.61	155	851	226.74	500

r_{HS}: hard-sphere diameter of silicon atom

K_{eq}: equilibrium constant for condensation reaction

S2 Identification of Polymerization Stages

The identification of polymerization stages is described in detail in our previous work (See Figure 6 of Ref. 1). In brief, we tracked the number of i) oligomers (silica cluster of size less than 4), ii) polymers (silica cluster of size more than 4), iii) oligomer-oligomer reaction, iv) ring formation reaction, and v) polymer-polymer reactions during polymerization. Based on the dominance of these parameters, we identified different stages of polymerization. The MC steps are scaled to real-time using scaling factor of 4.57×10^5 and 10.8×10^5 hr/MC steps for DS and CS systems. The protocol to obtain scaling factor is explained in Ref. 4. Since the order of the scaling factor is 5, the real-time value was reported with a precision of two decimal places.

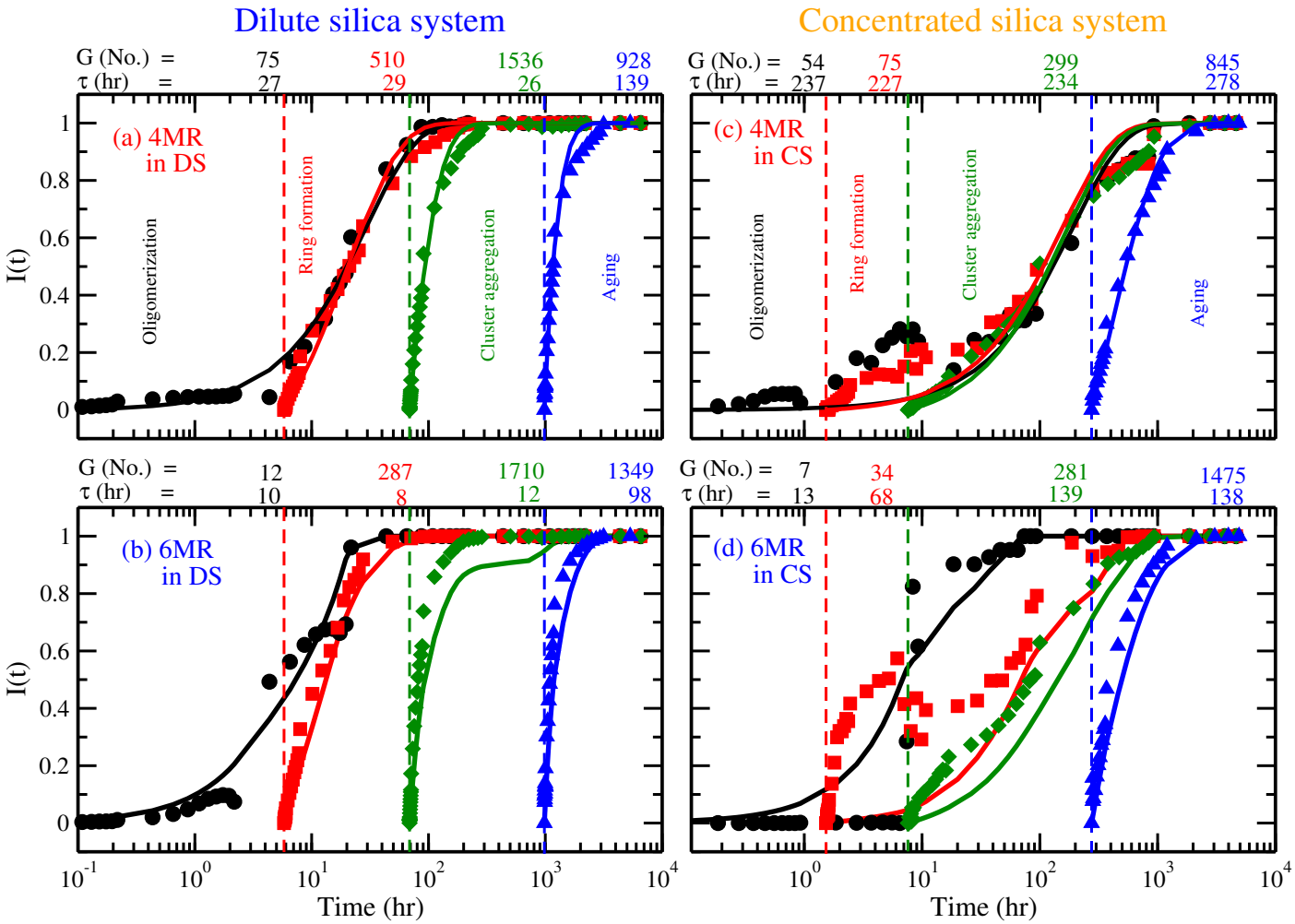

Figure S1: Representative curves showing fit of cumulative survival probability (I(t), symbols - raw data, lines fit to $I(t) = 1 - e^{-t/\tau}$) to obtain τ. (a,c) For 4MR, and (b,d) 6MRs formed during various stages of polymerization (oligomerization: black, ring-formation: red, cluster-aggregation: green, and aging: blue) in (a,b) DS and (c,d) CS systems.

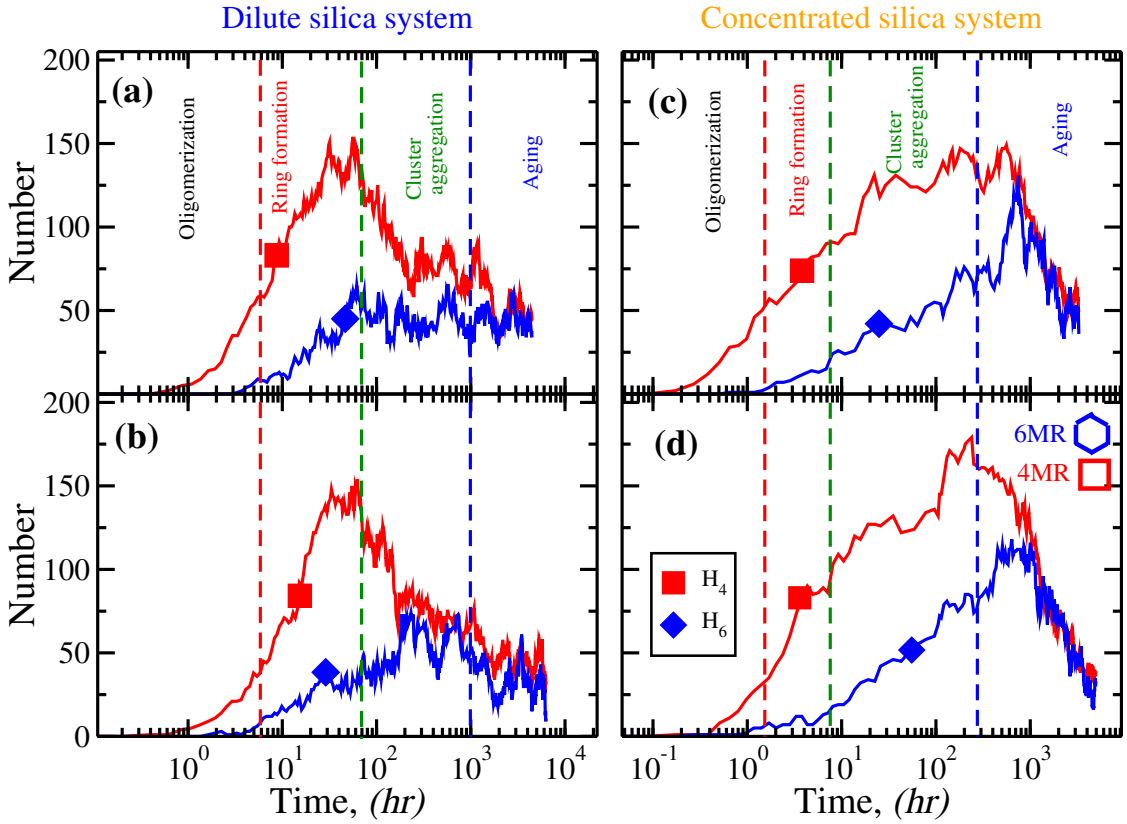

Figure S2: Evolution of four member ring (4MR−■) and six member ring (6MR−♦) in two duplicate systems for (a,b) DS and (c,d) CS system.

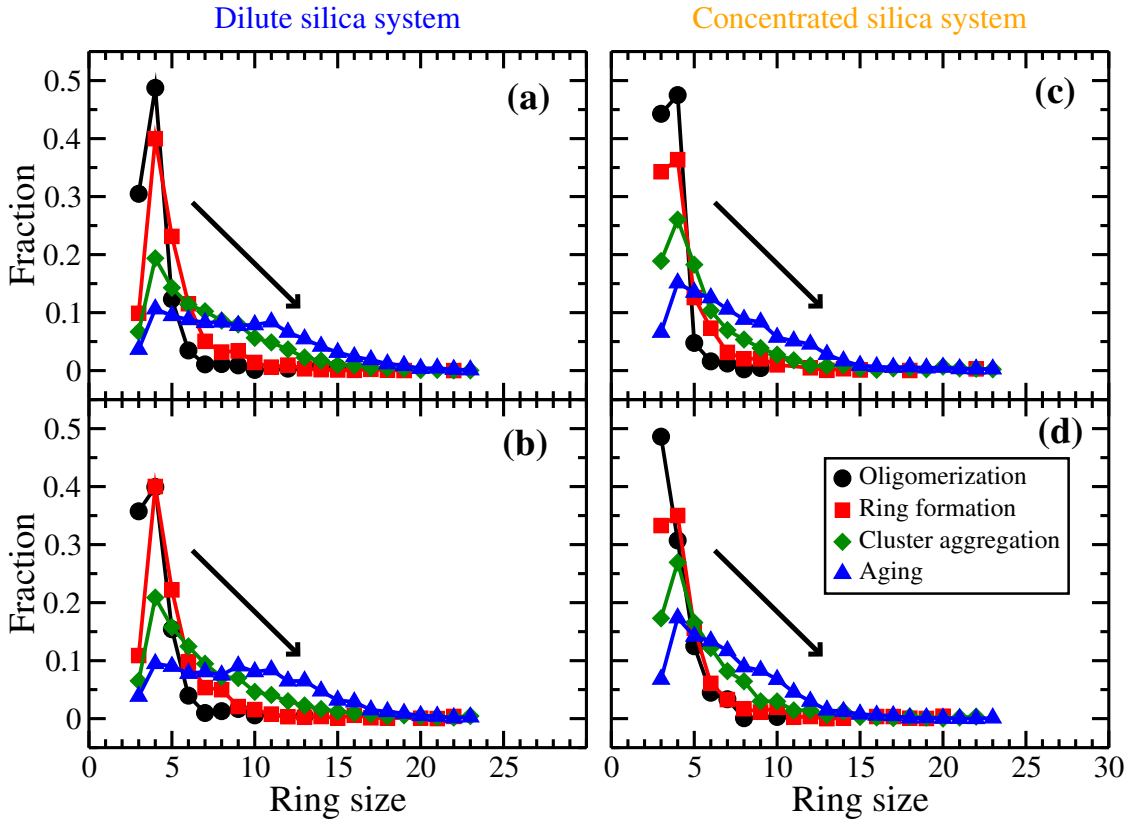

Figure S3: Data of ring size distribution in two duplicate systems of (a,b) DS and (c,d) CS systems.

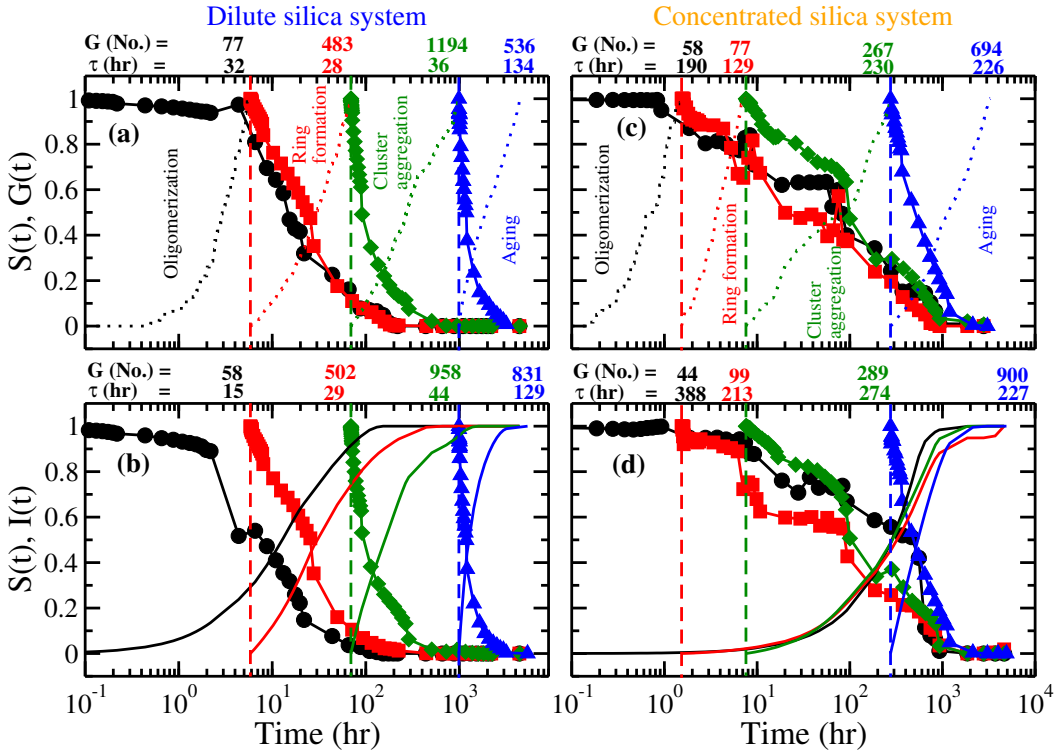

Figure S4: Data of survival probabilities (S(t)) of **4MR in two duplicate systems** of (a,b) DS and (c,d) CS systems. Normalized cumulative number of rings (G(t)- dotted lines shown for top row) and normalized cumulative survival probability (I(t)- solid line shown for bottom row) and S(t) are displaced along the x-axis such that $t = 0$ coincide with the starting of the stage. The numbers above show cumulative generation (G) and residence time (τ) of rings per stage.

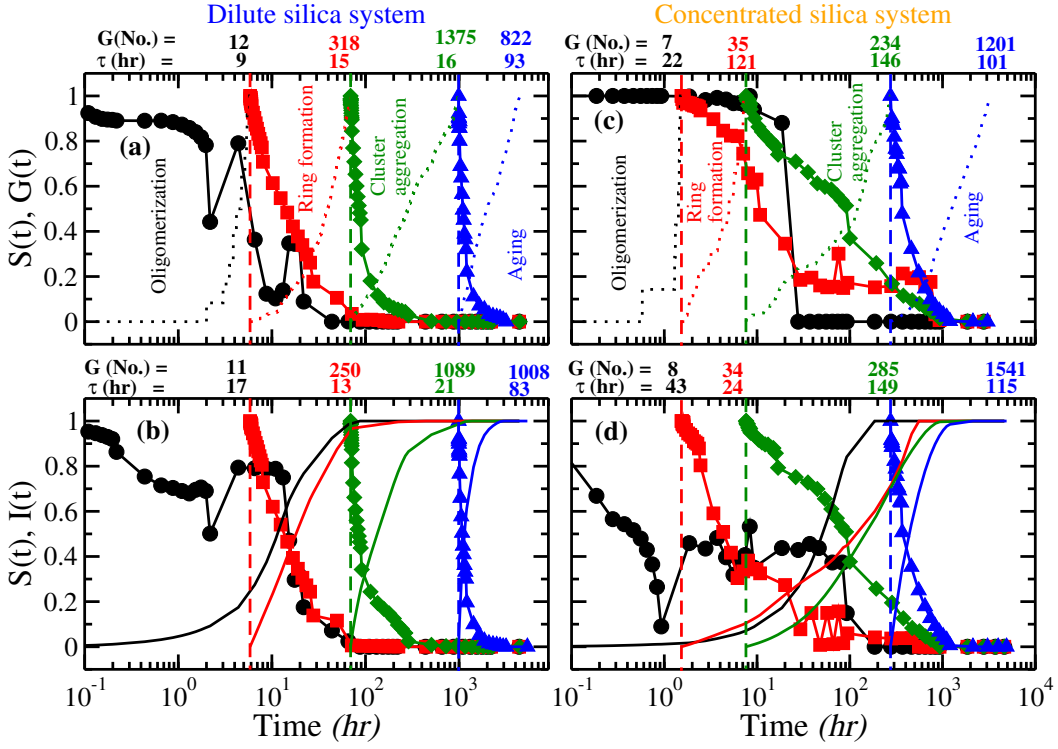

Figure S5: Same as Fig. S4 for 6MRs.

Table S2: Data of cumulative number of rings generated ($G_{iMR}, i = 4$ and 6) during various stages of polymerization for 3 similar systems studied.

	Dilute system				Concentrated system			
System No.	1	2	3	Avg.	1	2	3	Avg.
Stages	G_{4MR}							
Oligomerization	75	77	58	70 ± 6.03	54	58	44	52 ± 4.16
Ring-formation	510	483	502	498.333 ± 8.01	75	77	99	83.667 ± 7.69
Cluster-aggregation	1536	1194	958	1229.333 ± 167.79	299	267	289	285 ± 9.45
Aging	928	536	831	765 ± 117.87	845	694	900	813 ± 61.58
	G_{6MR}							
Oligomerization	12	12	11	11.667 ± 0.33	7	7	8	7.333 ± 0.33
Ring-formation	287	318	250	285 ± 19.66	34	35	34	34.333 ± 0.33
Cluster-aggregation	1710	1375	1089	1391.333 ± 179.45	281	234	285	266.667 ± 16.37
Aging	1349	822	1008	1059.667 ± 154.31	1475	1201	1541	1405.667 ± 104.09

Table S3: Data of residence time (τ) of 4MRs and 6MRs during various stages of polymerization in 3 similar systems studied.

	Dilute system				Concentrated system			
System No.	1	2	3	Avg.	1	2	3	Avg.
Stages	τ_{4MR}, (hr)							
Oligomerization	26.644	31.927	14.743	24.44 ± 5.08	236.854	190.409	388.242	271.84 ± 59.73
Ring-formation	28.664	28.017	28.637	28.44 ± 0.21	226.795	128.872	213.425	189.70 ± 30.66
Cluster -aggregation	25.633	36.36	43.569	35.19 ± 5.21	234.115	230.171	273.672	245.99 ± 13.89
Aging	139.362	133.818	129.473	134.22 ± 2.86	278.233	225.788	227.128	243.72 ± 17.26
	τ_{6MR}, (hr)							
Oligomerization	9.99	8.877	17.351	12.07 ± 2.66	13.475	22.261	42.634	26.12 ± 8.64
Ring-formation	8.451	14.703	13.423	12.19 ± 1.91	67.945	121.217	24.391	71.18 ± 28.0
Cluster -aggregation	12.406	16.344	20.865	16.54 ± 2.44	139.098	145.524	148.935	144.52 ± 2.88
Aging	98.33	92.916	82.948	91.40 ± 4.50	137.524	101.067	114.991	117.86 ± 10.62

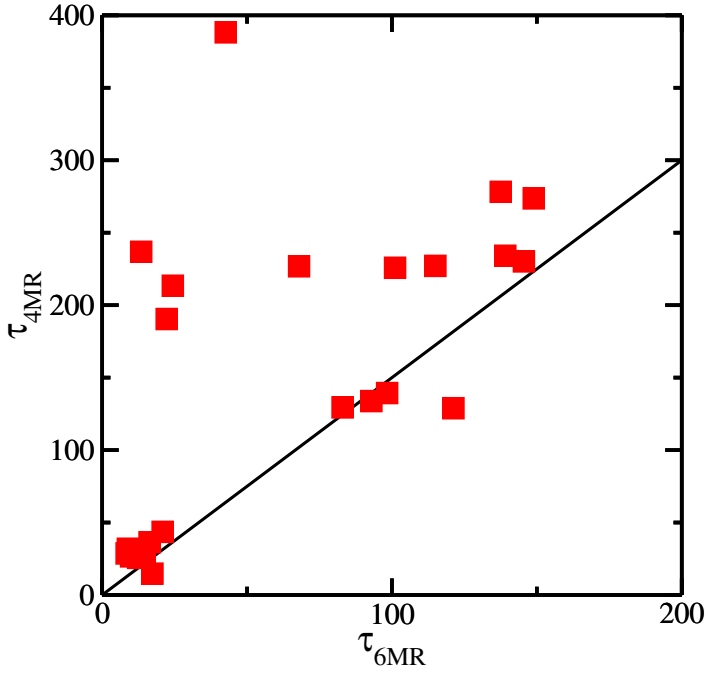

Figure S6: Parity plot showing survival times (τ) of 4MR (y-axis) and 6MR (x-axis) for all CS and DS system studied (Table S3) in various stages of polymerization. The solid line indicates the $\tau_{4MR} = 1.5\tau_{6MR}$

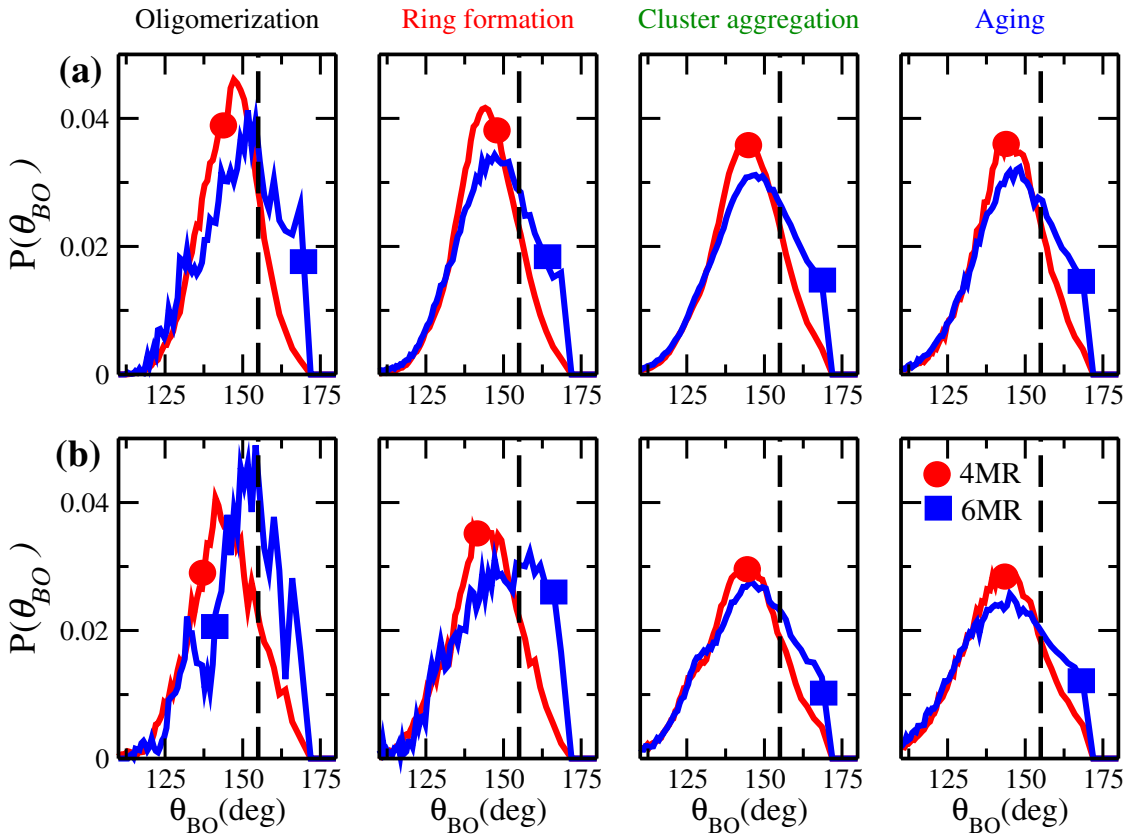

Figure S7: Probability distribution of Si-O-Si angle (θ_{BO}) formed on bridging oxygen between two connected tetrahedrons in 4MR (●) and 6MR (■) for (a - top row) DS and (b - bottom row) CS systems at various stages of polymerization. The vertical dash line at $\theta = 155°$ represents the equilibrium angle. Broad and distributed $P(\theta_{BO})$ is observed for 6MR compared to the narrow distribution of 4MR.

S3 Non-Gaussian Nature of Si-O-Si Angle Distribution

The reason for non-guassian distribution of $P(\theta_{BO})$ (Fig. S7) lies in the energy landscape of angle bending potential (U_A) as shown in Fig. S8. When value of θ increases beyond 180, we consider the smaller value (i.e., ϕ as per the convention of Fig. S8) in the simulation. This makes the energy landscape very broad, between 120-220 degrees. The inset of Fig. S8 shows the zoomed version around $\theta = 180$, where we see that the harmonic nature of the curve is maintained at around $\theta = \theta_0 = 155$. As per the equipartition theorem,[5,6] each degree of freedom will have $0.5k_BT$, but the peak height at $\theta = 180$ is only $0.4k_BT$. Thus, the Si-O-Si angle observes significant freedom beyond $\theta = 155$. At $\theta = 140$, the value of $U_A = 1k_BT$ and significant energy penalty is observed below $\theta = 140$. This is the reason that the most probable θ in $P(\theta)$ is at $\theta = 140$ and not equilibrium value of 155. From the snapshots of the system, we observed that 4MR form a constrained planner geometry, whereas 6MR has a flexible ring shape. The breaking of 6MR provides relaxation of a pentamer with (more degrees of freedom via the bond and angle bending), whereas these degrees of freedom are lesser when a 4MR breaks. Though 4MR are strained, their breakage does not help in alleviating the strain on the cluster; rather, breaking of 6MR does. Thus the continuous breaking, re-forming and relaxation of 6MR leads to a shoulder in $P(\theta_{B0})$ at larger values of θ, suggesting that 6MRs are significantly flexible.

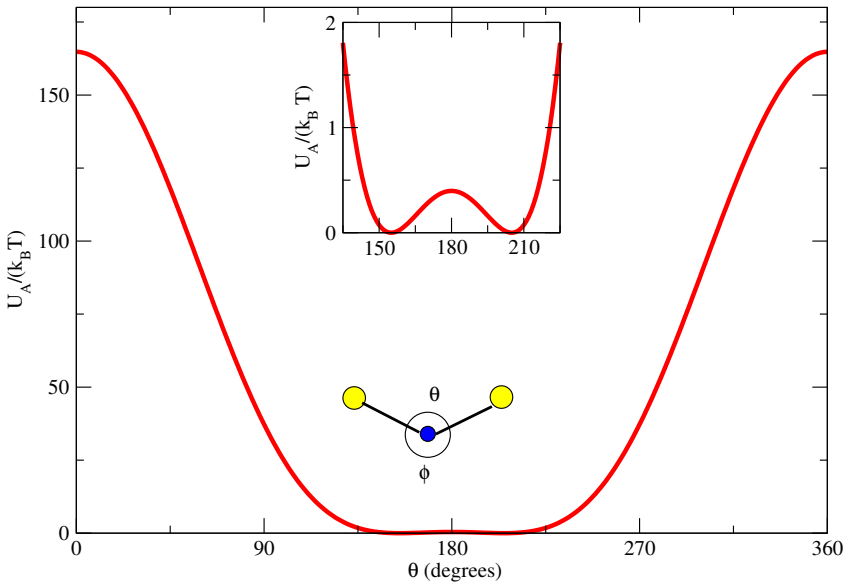

Figure S8: Variation of angle bending energy ($U_A = 0.5k_A(\cos\theta - \cos\theta_0)^2$) with respect to angle θ. Here θ and ϕ are Si-O-Si angles measured from top and bottom side. $\theta + \phi = 360$.

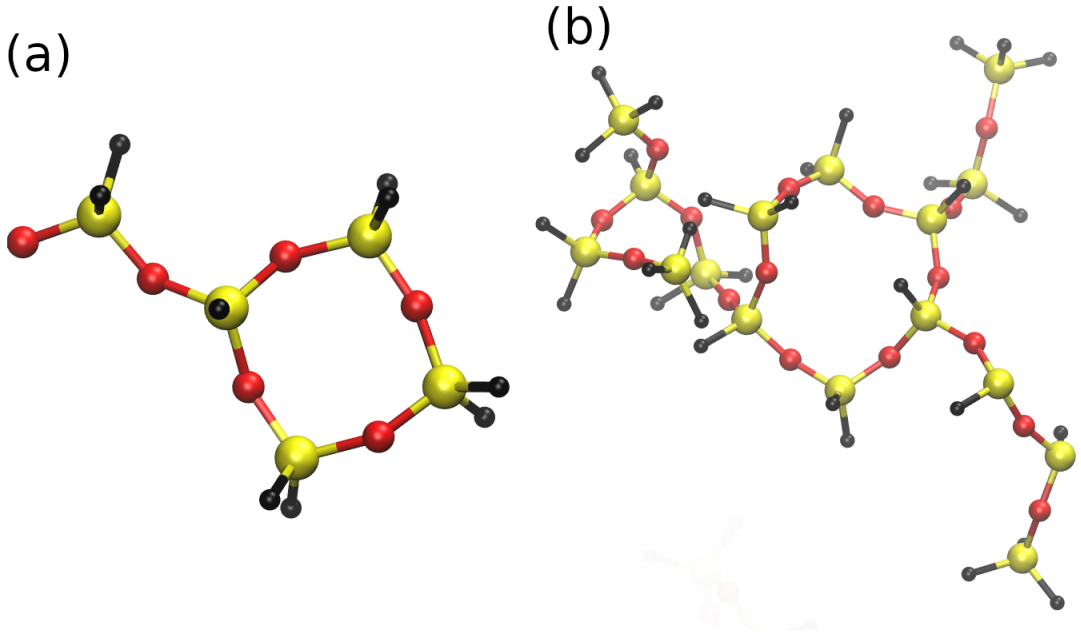

Figure S9: Snapshot of (a) 4MR and (b) 6MR observed during simulation. The Si-O-Si angles in 4MR are more uniform and ring lies in a plane whereas the Si-O-Si angles in 6MR have large variations and the ring does not lies in the plane.

Table S4: Computational strategy used to identify different reaction events

Scenarios	$\theta_i(t_1)$	$\Phi_i(t_1)$	$\theta_i(t_2)$	$\Phi_i(t_2)$	Reaction
1	0	0	1	1	IR generated via $O2I_f$
2	0	0	1	0	GR generated via $G2G_f$
3	1	1	0	0	IR broken via $O2I_b$
4	1	1	1	1	IR survived - no reaction
5	1	1	1	0	IR to GR via $I2G_f$
6	1	0	0	0	GR breaking via $G2G_b$
7	1	0	1	1	GR to IR via $I2G_b$
8	1	0	1	0	GR survived - no reaction

$\theta_i = 1$ if i^{th} ring exist, else 0

$\Phi_i = 1$ if i^{th} ring is isolated ring (IR) and 0 if grouped ring (GR)

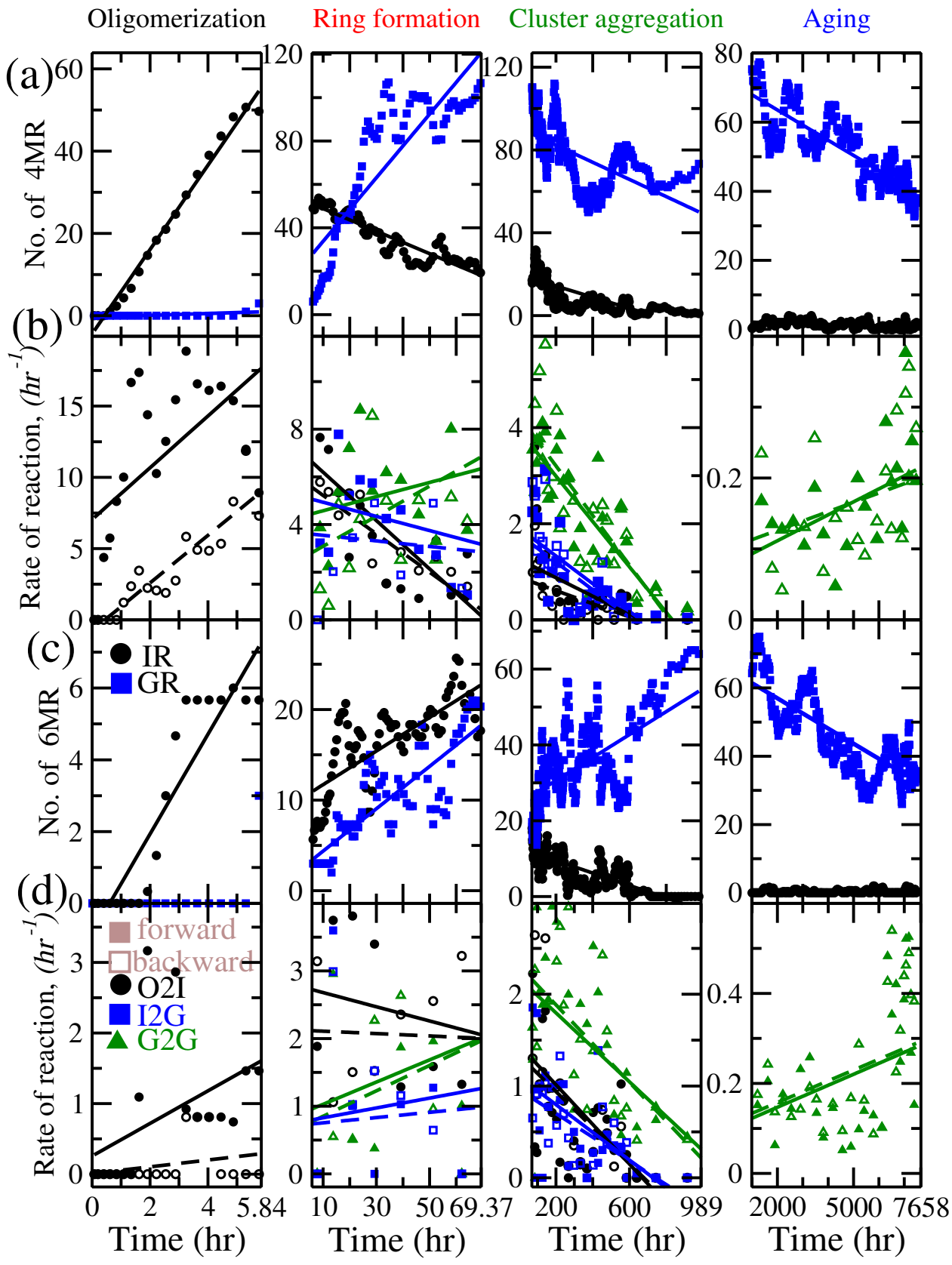

Figure S10: Variation in number of (a) 4MR and (c) 6MRs (IR - • and GR - ■) with respect to time in **DS system** during various stages of polymerization. Solid lines in subfigure a,c are linear fit to number of rings, but no parameters were calculated. Reaction rates of (b) 4MR and (d) 6MR formation (solid symbol) and breaking (open symbol) via O2I (•), I2G(■), and G2G(▲) reactions. Solid and dotted lines in subfigure b,d are linear fit to formation and breaking reaction rates. The slope (m) and intercept (r_0) parameters were calculated and given in Table S5.

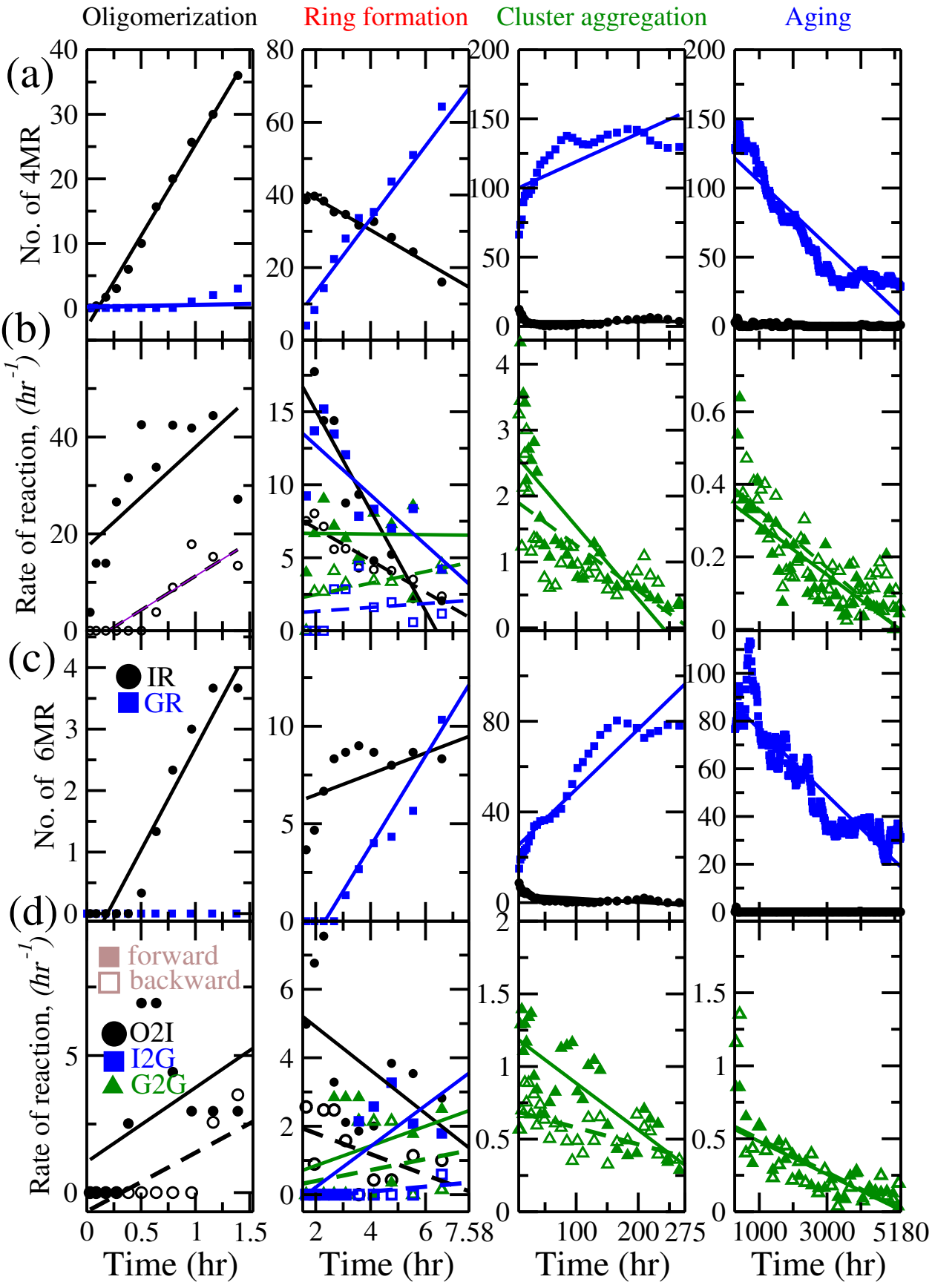

Figure S11: Number and reactions rates of 4MR and 6MR for **CS system**. Legends are same as Fig. S10. The values of m and r_0 obtained are reporeted in Table S6.

Table S5: Fitting parameters (m-slope and r_0-intercept) of various ring formation and breaking reaction rates for the **DS system**

Reactions		$O2I_f$	$O2I_b$	$I2G_f$	$I2G_b$	$G2G_f$	$G2G_b$
Stages					4MR		
Oligomerization	m (hr^{-2})	1.816	1.668	0	0	0	0
	r_0 (hr^{-1})	7.044	-0.741	0	0	0	0
Ring-formation	m (hr^{-2})	-0.101	-0.081	-0.030	-0.012	0.030	0.063
	r_0 (hr^{-1})	6.619	5.559	5.059	3.597	4.454	2.824
Cluster-aggregation	m (hr^{-2})	-0.002	-0.001	-0.003	-0.003	-0.005	-0.005
	r_0 (hr^{-1})	1.127	0.788	1.706	1.576	3.609	3.880
Aging	m (hr^{-2})	0	0	0	0	1.83×10^{-5}	1.31×10^{-5}
	r_0 (hr^{-1})	0	0	0	0	0.093	0.113
					6MR		
Oligomerization	m (hr^{-2})	0.231	0.048	0	0	0	0
	r_0 (hr^{-1})	0.258	0.009	0	0	0	0
Ring-formation	m (hr^{-2})	-0.010	-0.002	0.007	0.004	0.016	0.019
	r_0 (hr^{-1})	2.724	2.117	0.798	0.738	0.960	0.774
Cluster-aggregation	m (hr^{-2})	-0.002	-0.002	-0.002	-0.001	-0.002	-0.002
	r_0 (hr^{-1})	1.297	1.197	0.995	0.869	2.043	2.161
Aging	m (hr^{-2})	0	0	0	0	2.44×10^{-5}	2.40×10^{-5}
	r_0 (hr^{-1})	0	0	0	0	0.122	0.133

Table S6: Fitting parameters of reaction rates for the **CS system**

Reactions		$O2I_f$	$O2I_b$	$I2G_f$	$I2G_b$	$G2G_f$	$G2G_b$
Stages		4MR					
Oligomerization	m (hr^{-2})	20.655	14.053	0	0	0	0
	r_0 (hr^{-1})	17.256	-2.785	0	0	0	0
Ring-formation	m (hr^{-2})	-3.428	-1.091	-1.703	0.132	-0.021	0.394
	r_0 (hr^{-1})	16.699	7.526	13.511	1.269	6.674	2.288
Cluster-aggregation	m (hr^{-2})	0	0	0	0	-0.011	-0.007
	r_0 (hr^{-1})	0	0	0	0	2.563	1.894
Aging	m (hr^{-2})	0	0	0	0	-7.001×10^{-5}	-7.97×10^{-5}
	r_0 (hr^{-1})	0	0	0	0	0.341	0.387
		6MR					
Oligomerization	m (hr^{-2})	2.713	2.142	0	0	0	0
	r_0 (hr^{-1})	1.116	-0.690	0	0	0	0
Ring-formation	m (hr^{-2})	-0.634	-0.303	0.598	0.073	0.288	0.161
	r_0 (hr^{-1})	5.204	1.934	-0.067	-0.095	0.711	0.321
Cluster-aggregation	m (hr^{-2})	0	0	0	0	-0.003	-0.001
	r_0 (hr^{-1})	0	0	0	0	1.183	0.686
Aging	m (hr^{-2})	0	0	0	0	-1.13×10^{-4}	-1.14×10^{-4}
	r_0 (hr^{-1})	0	0	0	0	0.564	0.581

S4 Kinetics of 6MR Formation and Breaking in the CS System

The effect of silica precursor concentration on the evolution of bigger (6MR) rings is obtained by comparing the evolution of 6MR in the CS system with 1) 6MR of the DS system and 2) 4MR of the CS system. Further to understand the role of silica precursor concentration on collective evolution of smaller and bigger rings, we compared 3) 6MR vs 4MR of CS system with 6MR vs 4MR of DS system. We describe these comparisons, in brief, one after another.

S4.1 Comparison of Kinetics of 6MR in CS with 6MR of DS System:

Since the duration of polymerization stages of DS and CS systems are different, we calculated the difference of kinetic parameters Δm and Δr_0 as shown in Fig. S12. We observe that the rates of isolated

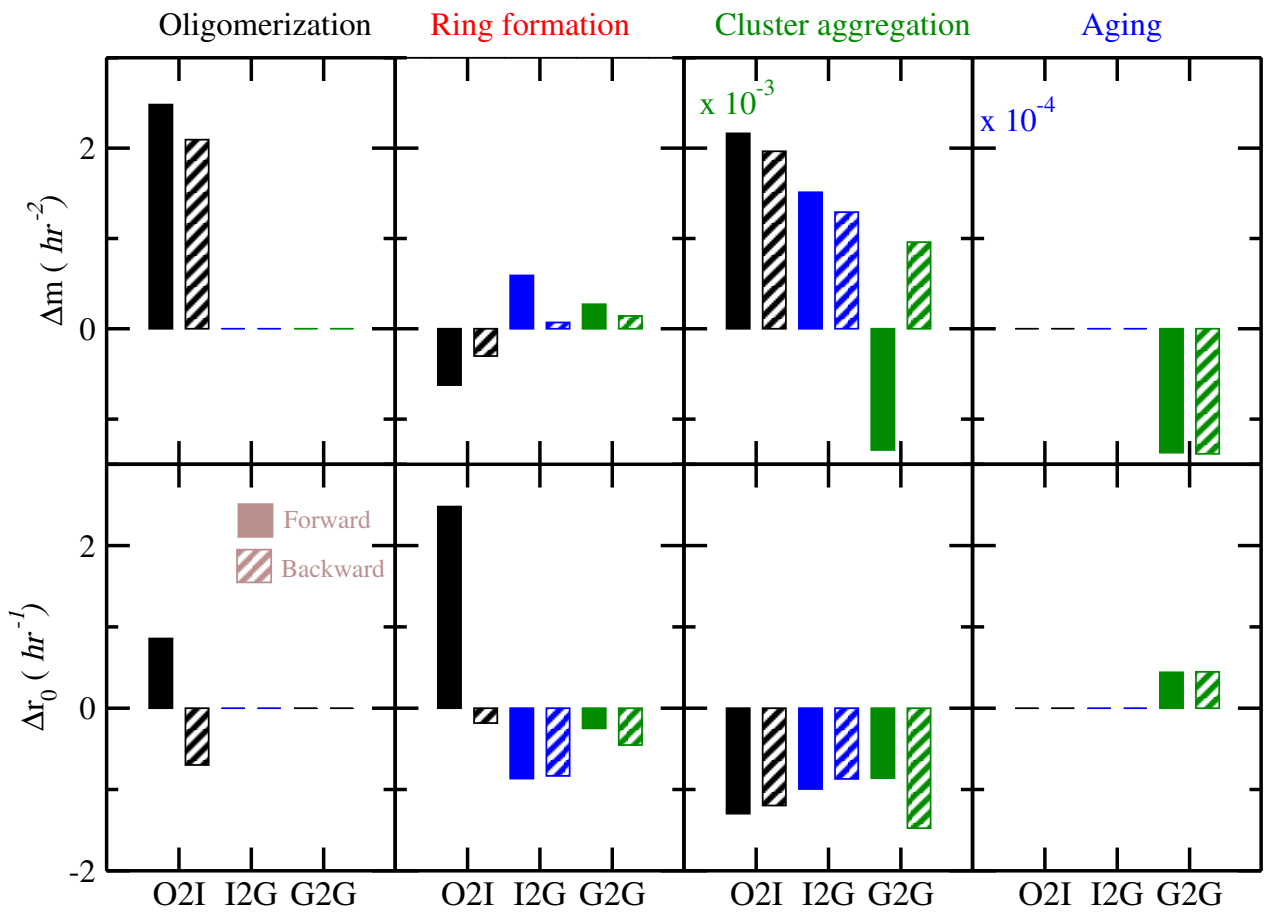

Figure S12: The difference in the fitting parameters (top row - Δm and bottom row - Δr_0) of reaction rates for 6MR formation (solid bar) and breaking (striped bars) in CS vs DS systems.

6MR formation and breaking via O2I reactions in the CS system are significantly higher than the DS system because of the faster kinetics of condensation reaction leading to the more and quicker formation of larger oligomers (to form 6MRs). However, once larger oligomers have formed during the ring-formation stage, the IR formation decreases ($\Delta m < 0$), and GRs formation increases; however, reactions rates in the CS system are similar to that of the DS system ($\Delta m \sim 0$). During the cluster-aggregation, we observed that mostly G2G formation and breaking reactions occur in the CS system (Fig. S11), whereas, other reactions were also occurring in the DS system (Fig. S10). As a result, we observe $\Delta m > 0$ for the cluster-aggregation stage. Although $\Delta m \sim 0$, however, the larger duration of the cluster-aggregation stage suggests that the rates are non-zero in this and later stages. We further observe that during aging, the formation and breaking rates are almost similar; however, the trends are decreasing for the CS system, suggesting lesser re-organization of the cluster in the CS system, whereas continuous re-organization in the DS system.

S4.2 Comparison of Kinetics of 6MR with 4MR in the CS System:

Since we are comparing the evolution of 4MR and 6MR for the same system, we directly calculated the Δr. Due to the decreased propensity of hydrolysis reaction in the CS system, the breaking event of 6MR

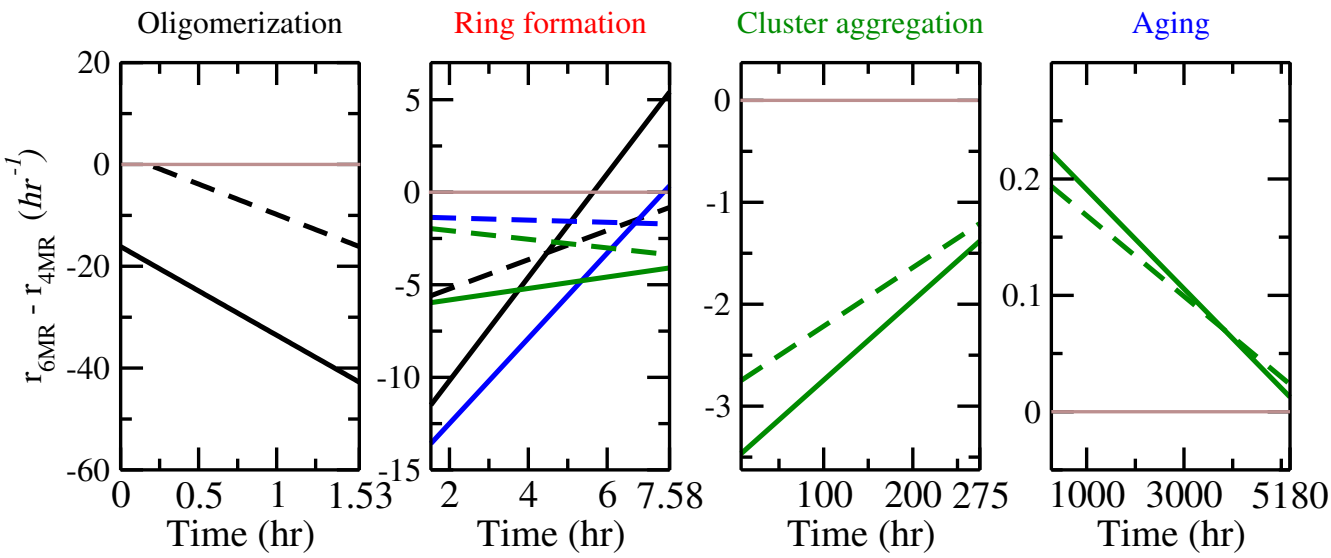

Figure S13: Difference between 6MR and 4MR reaction rates in the CS system for O2I (black lines), I2G (blue lines), and G2G (green lines) reactions (formation: solid lines and breaking: dashed lines) in various stages of polymerization.

is lesser than 4MR and starts at around 0.5 hr in the oligomerization stage. During the ring-formation stage, the absolute rates of 6MR reactions (both formation and breaking) are significantly lesser compared to 4MRs, while the trends for the formation of 6MRs are increasing. In the cluster-aggregation stage, the total number of 6MRs formed are lesser compared to 4MR; thus, its breaking events are lesser, and as a result, the absolute rates of 6MR (formation and breaking) are lesser (i.e., $\Delta r < 0$) compared to 4MRs. During the aging stage, we observed that the re-organization of 6MR is slightly higher than 4MR, as evident from higher rates of G2G (formation and breaking) reactions.

S4.3 Comparison between 6MR vs 4MR of the CS system and 6MR vs 4MR of the DS system:

The difference in the evolution of smaller and bigger rings at different concentrations is illustrated via the calculation of O2I, I2G, and G2G (formation and breaking) reaction rates, as shown in Fig. 10 of main manusript and S13. The overall behavior is qualitatively similar, suggesting no significant change in the evolution of smaller and bigger rings occurs with changes in concentrations. Few noteworthy quantitative observations are; 1) lesser formation of 6MR in the CS system compared to the DS system, 2) lesser breaking events of 6MR (i.e., higher residence time) during oligomerization compared to the DS system, 3) 6MR formation and breaking in the DS system via O2I reactions are higher compared to 4MR, whereas all reaction rates of 6MR are lesser compared to 4MR in the CS system, and 4) mostly GRs are formed via G2G (formation and breaking) reactions in the CS system during cluster-aggregation, and remaining significant rates of other reactions are also observed in the DS system. These observations

could be understood from the fact that the kinetics of condensation and hydrolysis reactions become faster and slower, respectively, at higher silica precursor concentrations. Thus, the re-organization is significantly decreased, reflected in the higher residence times, resulting in the lesser rates of ring breaking reaction. Further, we observe that in the DS system, the rates of ring formation and breaking reactions are comparable, whereas significant differences are observed between rates of formation and breaking reaction in the CS system, highlighting the significant push towards the formation of Si-O-Si bonds.

References

[1] Shere, I.; Malani, A. Polymerization kinetics of a multi-functional silica precursor studied using a novel Monte Carlo simulation technique. *Phys. Chem. Chem. Phys.* **2018**, *20*, 3554.

[2] Malani, A.; Ayappa, K. G. Relaxation and jump dynamics of water at the mica interface. *J. Chem. Phys.* **2012**, *136*, 194701.

[3] Malani, A.; Auerbach, S. M.; Monson, P. A. Monte Carlo simulations of silica polymerization and network formation. *J. Phys. Chem. C* **2011**, *115*, 15988.

[4] Shere, I.; Malani, A. Porosity development in silica particles during polymerization: Effect of solvent reactivity and precursor concentration. *J. Phys. Chem. C* **2020**, *124*, 520.

[5] McQuarrie, D. A. *Statistical Mechanics*; Viva Books Private Limited: New Delhi, 2003.

[6] Allen, M. P.; Tildesley, D. J. *Computer simulation of liquids*; Oxford University Press: New York, USA, 1987.